International Journal of Microwave and Wireless Technologies

cambridge.org/mrf

Design of ultra-wideband antenna based on one-dimensional convolutional neural network

Pengcheng Gao[1], Weigang Wang[1], Yuanjian Liu[1], Qijian Liu[1], Yonghao Chen[1] and Xiangming Yan[2]

[1]College of Electronic and Optical Engineering & College of Flexible Electronics (Future Technology), Nanjing University of Posts and Telecommunications, Nanjing, Jiangsu, China and [2]Portland Institute, Nanjing University of Posts and Telecommunications, Nanjing, Jiangsu, China

Research Paper

Cite this article: Gao P, Wang W, Liu Y, Liu Q, Chen Y, Yan X (2025) Design of ultra-wideband antenna based on one-dimensional convolutional neural network. *International Journal of Microwave and Wireless Technologies* **17**(3), 482–491. https://doi.org/10.1017/S1759078725000303

Received: 20 August 2024
Revised: 9 February 2025
Accepted: 27 February 2025

Keywords:
band notched; bent slot structure; one-dimensional convolutional neural network; ultra-wideband antenna

Corresponding author: Weigang Wang; Email: wangwg2020@163.com

Abstract

This paper presents a notched ultra-wideband antenna designed to suppress interference from narrowband communication systems. The antenna features a defected ground structure and a stepped microstrip feedline for improved impedance matching and enhanced bandwidth. A bent slot structure is incorporated into the radiating patch to achieve the band-notched characteristic. It has a wide tunable frequency range which allows for flexible adjustment of the notch frequency. Traditional optimization methods, such as numerical analysis, are computationally expensive and inefficient, while heuristic algorithms are less precise. To address these challenges, an improved one-dimensional convolutional neural network (1DCNN-IPS) model is proposed for optimizing the bent slot design more efficiently. The trained 1DCNN-IPS model can accurately predict the antenna's electromagnetic parameters, reducing mean squared error and training times compared to traditional methods. This provides an efficient and precise solution for antenna structural optimization.

Introduction

With the development of wireless communication technology, ultra-wideband (UWB) has a wide range of application prospects in wireless sensor networks and indoor localization [1–3]. The UWB communication system works in the frequency band of 3.1–10.6 GHz, which is inevitably interfered with by the narrowband communication band [4, 5]. Currently, the simplest way to suppress interference is to design UWB antennas with band-notched characteristics [6]. In this way, the antenna is equivalent to adding a band-rejection filter [7]. The main methods to realize the antenna band-notched characteristics included cutting slots in the radiating patch and microstrip feedline [8–10], loading parasitic units on the radiating patch [11–13], loading slot structures on the ground plane [14, 15], etc. The advantages of these methods were that they are simple in structure and easy to design. However, these approaches increased the number of parameters in the antenna modeling process. Simulation software such as High Frequency Structure Simulator (HFSS) and Computer Simulation Technology (CST) consumes a lot of computational resources and increases the time cost in multivariate antenna optimization. To address this problem, scholars have trained the relationship between antenna structure parameters and reflection coefficient using ANNs. Literature [16] attempted to model the nonlinear relationship between antenna geometrical parameters and electromagnetic parameters by using a combination of artificial neural network (ANN) and simulated annealing algorithm. However, it used a smaller dataset, which led to lower fitting accuracy. Literature [17] utilized a multilayer perceptron (MLP) to fit the dimensional parameters of the model bends to the reflection coefficient parameters, but the model training was still slow. Literature [18] successfully estimated the resonant frequency of a rectangular microstrip antenna by employing ANNs and the method of moments. This approach reduced the computational complexity. However, during the training process, the model still had to face the issue of vanishing gradients.

In this paper, to meet the bandwidth requirements of UWB antennas, we first design a stepped microstrip-line structure. Then we integrate it with an inverted convex-shaped slot defected ground structure (DGS), which improves the impedance matching of the antenna and effectively increases the bandwidth of the antenna. To introduce a notch characteristic in the WiMAX frequency band, we employed a bent-slot design on the antenna surface. However, during antenna structure optimization, we found that traditional methods, such as numerical analysis, are hindered by high computational cost and low efficiency, while heuristic algorithms struggle with insufficient accuracy. In contrast, Convolutional Neural Networks (CNNs) can

© The Author(s), 2025. Published by Cambridge University Press in association with The European Microwave Association.

effectively capture the nonlinear relationship between device structure parameters and electromagnetic responses. To accelerate the optimization process of the bent slot structure, we proposed a one-dimensional convolutional neural network (1DCNN-IPS) model for optimizing the notch structure of the UWB antenna. Unlike traditional 1DCNNs, we optimized its propagation structure by introducing padding operations in the convolution layers, adding batch normalization (BN) layers after the convolution layers, and using ReLU activation functions between convolution layers. These improvements enabled the 1DCNN-IPS model to train data more efficiently and accurately describe the relationship between geometric parameters and electromagnetic responses in antenna design. Finally, we applied the 1DCNN-IPS model to accelerate the optimization process of the bent slot structure, successfully establishing a nonlinear mapping between the bent slot structure parameters and the reflection coefficient, thereby achieving the notch characteristic in the WiMAX frequency band (3.3–3.8 GHz). Experimental results show that the trained 1DCNN-IPS model can accurately describe the complex relationship between geometric parameters and antenna reflection coefficients, significantly reducing the time and computational complexity in the antenna design process. This method provides an efficient and precise solution for structural optimization in antenna design.

Antenna design simulation and characterization

The antenna designed in this paper is shown in Fig. 1. It is printed on the FR4 substrate and consists of a hexagonal radiating patch, a stepped microstrip feedline, and a DGS structure.

The microstrip line of the antenna is a stepped feedline with 50-Ω impedance. The impedance of 50-Ω can reduce reflections, signal loss, and signal distortion. The microstrip line characteristic impedance can be computed by

$$\varepsilon_{re} = \frac{\varepsilon_r + 1}{2} + \frac{\varepsilon_r - 1}{2}\left(1 + 12\frac{h}{W}\right)^{-\frac{1}{2}}, \quad (1)$$

$$Z_0 = \frac{120\pi}{\sqrt{\varepsilon_{re}}\left[\frac{W}{h} + 1.393 + 0.667\ln\left(\frac{W}{h} + 1.444\right)\right]}, \quad (2)$$

where W denotes the width of the microstrip line and h represents the height of the dielectric substrate. ε_r is the relative permittivity of the dielectric substrate. ε_{re} represents the effective relative permittivity of the microstrip line, and Z_0 represents the characteristic impedance of the microstrip line. After the above calculations, we can estimate the microstrip line width. Other structural parameters of the antenna are shown in Table 1.

The design evolution of the antenna structure is shown in Fig. 2. The antenna is simulated by using HFSS to measure the return loss of the antenna, which is calculated by

$$\Gamma = \frac{Z_o - Z_{in}}{Z_o + Z_{in}}, \quad (3)$$

$$RL = -20log(|\Gamma|). \quad (4)$$

Z_o and Z_{in} represent the characteristic impedance of the transmission line and the input impedance of the feedline, respectively. Γ is the reflection coefficient of the antenna. The smaller the reflection coefficient is, the better the impedance matching will be. The return loss is a method of representing the reflection coefficient in logarithmic form (dB), and $|S_{11}| < -10$ dB is usually used as a criterion for antenna bandwidth in engineering applications [19].

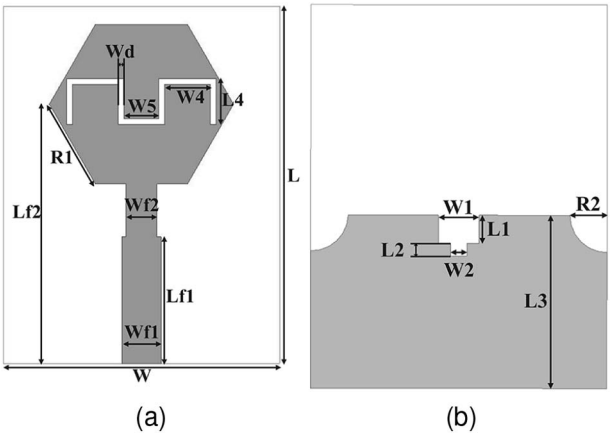


Figure 1. Structure of the UWB antenna: (a) top view and (b) bottom view.

Table 1. Dimensions of the antenna

Parameter	Value (mm)	Parameter	Value (mm)
W	24	R2	3
L	31	H	1.5
R1	8	W1	3.3
Wf1	3.4	L1	2.3
Wf2	2.7	W2	1.3
Lf1	11	L2	1
Lf2	22.5	L3	14

The reflection coefficient of the four antenna configurations is shown in Fig. 3. As we can see, the bandwidth of Structure 1 is 3.3–8.7 GHz. Quarter-circle slots are cut in the corners of the ground plate of Structure 1, which are used to build Structure 2. Invert convex shape slots are cut in the middle of Structure 2, and we can get Structure 3. In these ways, the antenna surface current path is enlarged and the impedance matching characteristics are improved [20]. The antenna's bandwidth increased to 3.2–9.2 GHz and 3.2–20 GHz, respectively. Finally, the rectangular microstrip feedline in Structure 3 is changed to a stepped shape. This modification further increases the antenna's bandwidth and enables it to satisfy the UWB standard in the low-frequency band. The low frequency of Structure 4 is 2.95 GHz.

The bandwidth covered by UWB antennas ranges from 3.1 GHz to 10.6 GHz. Within this range, there are narrowband commercial frequency bands such as WiMAX (3.3–3.8 GHz), C-band satellite communication (3.7–4.4 GHz), and digital microwave communication (4.3–4.5 GHz), which may interfere with the frequency bands of UWB antennas. To address the issue of frequency reuse, enhance spectrum efficiency, and minimize costs wherever possible, we have designed UWB antennas with band-notched properties within the WiMAX frequency band. Cut slots in the radiating patch enable the antenna to achieve band-notched characteristics. The band notch is implemented by using the following formulas [21]:

$$f_n = \frac{c}{2L_s\sqrt{\varepsilon_{re}}}, \quad (5)$$

$$\varepsilon_{re} = \frac{\varepsilon_r + 1}{2}, \quad (6)$$

https://doi.org/10.1017/S1759078725000303 Published online by Cambridge University Press

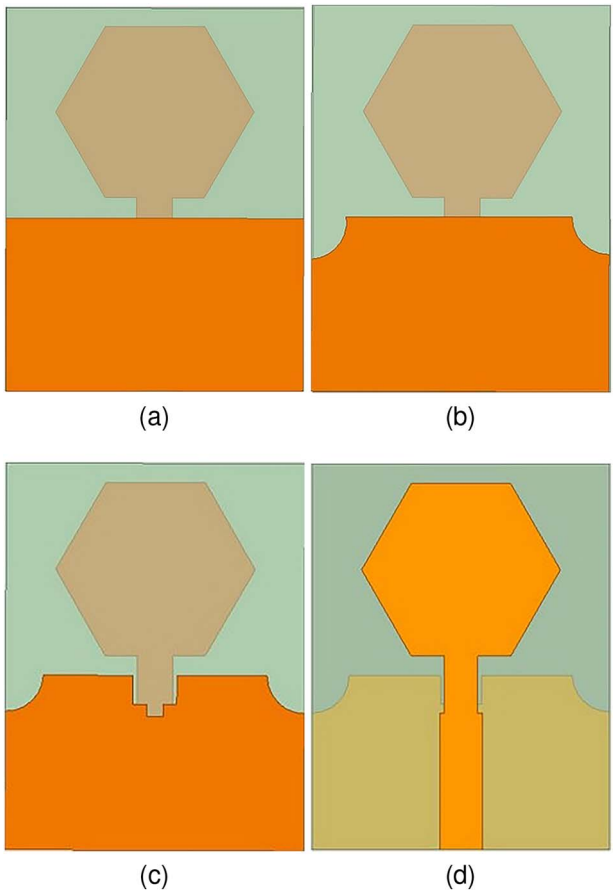


Figure 2. The design evolution of the antenna structure: (a) structure 1, (b) structure 2, (c) structure 3, and (d) structure 4.

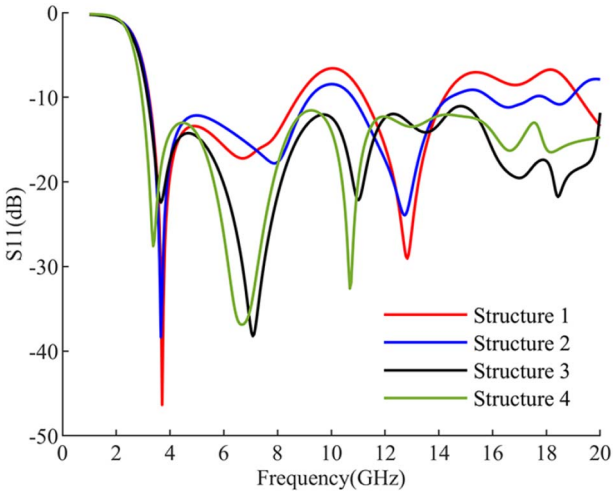


Figure 3. The S11 parameters of four antenna structures.

where f_n is the resonant frequency and L_s is the length of the slot.

The inner perimeter length of the slot required to produce a notch at 3.6 GHz can be estimated using (5) and (6). A bent slot is made on the radiating patch to facilitate the opening of the slot inside the hexagonal radiating patch and increase the adjustment space. The bent slot enables the work current to be concentrated at the edge of the thin slot, so the nearby currents have the same amplitude and opposite direction. As a result, the radiated electromagnetic energies counteract each other in the far-field region and form the band-rejected characteristic. Figure 4 shows the reflection coefficients corresponding to different inner perimeters of the bent slot.

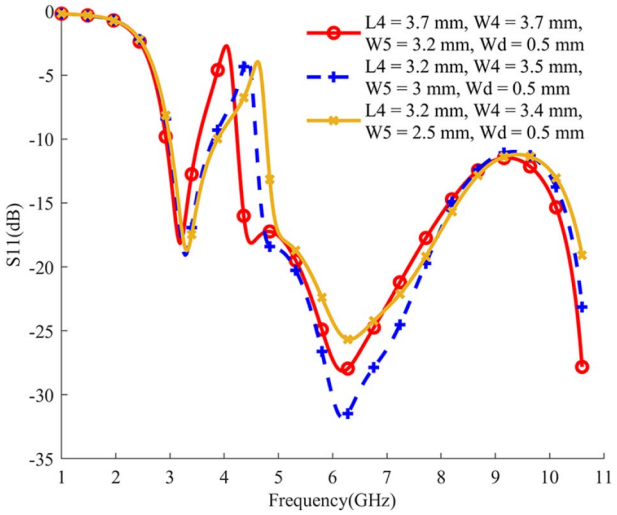


Figure 4. Input reflection coefficients corresponding to different lengths of antenna bent slot.

From Fig. 4, it can be seen that the size of the antenna bent slot parameter affects the range of the notched band. By optimizing the structural parameters, we can achieve the band-notched characteristic in WiMAX (3.3–3.8 GHz) of the antenna. However, using HFSS for antenna parameter optimization consumes a significant amount of resources and needs high computational costs. Fortunately, the neural network can get a nonlinear relationship between input and output in a short time after the training is completed. This approach can significantly reduce design time. Based on this, the following 1DCNN-IPS model is set up to optimize the UWB antenna.

Improved one-dimensional convolutional neural network

The traditional method for optimizing antenna structures relies on the optimization function of electromagnetic simulation software, but each optimization process consumes a great deal of time. Compared with traditional methods, 1DCNN can automatically learn features and show better performance when processing large-scale data.

1DCNN

CNN [22–24] structure has been widely used in recent years. Its structure consists of multiple layers like the convolutional layer, pooling layer, and fully connected layers, as shown in Fig. 5, which is the network structure of a 1DCNN. Compared to heuristic optimization techniques such as genetic algorithms and particle swarm optimization, ANNs possess powerful learning capabilities and excellent nonlinear mapping abilities. Once the relationship between antenna structural parameters and reflection coefficient is established, even minor adjustments to the antenna structure can immediately yield the corresponding antenna performance without the need for additional inference calculations.

https://doi.org/10.1017/S1759078725000303 Published online by Cambridge University Press

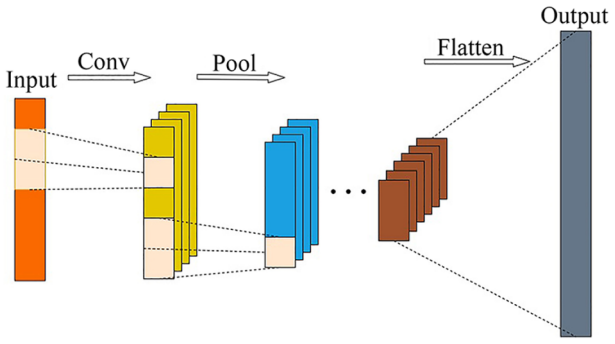


Figure 5. 1DCNN architecture.

Convolutional layers

The convolutional layer can extract edge features and deeper feature information from the image. It consists of multiple layers of convolutional kernels of the same size. In the antenna modeling process, the structural parameters of the antenna can be abstracted as a one-dimensional image and then processed with the convolutional layer. The operation of the convolutional layer is evaluated by

$$O^l = \sum_{i=1}^{n} \sum_{j=1}^{m} I_{i,j}^{l-1} \times K_{i,j}^{l} + b^l, \tag{7}$$

where I^{l-1} represents the input of the convolutional layer in layer $l-1$. O^l represents the output of the convolutional layer in layer l. K^l represents the convolutional kernel in layer l, and b^l is the bias of the convolutional kernel in layer l.

Pooling layer

The main role of the pooling layer is to reduce the dimensionality of the data by downsampling the input data and to retain the key information from the input data. The max pooling layer and average pooling layer are commonly used for pooling in CNN and can be expressed as

$$(s_j)_{\max} = \max_{i \in R_j} a_i, \tag{8}$$

$$(s_j)_{\text{avg}} = \frac{1}{|R_j|} \sum_{i \in R_j} a_i, \tag{9}$$

where a_i is the i-th element in the j-th region R_j.

Fully connected layer

The fully connected layer can synthesize all the extracted features and then map them to labels for regression prediction. The operation of the fully connected layer can be written as

$$y^r = f(w^r \bullet y^{r-1} + b^r), \tag{10}$$

where y^r is the output of the r-th fully connected layer and w^r is the weight matrix. b^r is the bias entry.

Loss function

The loss function represents the extent to which the prediction falls short of the actual data. Through a backpropagation algorithm, CNN can calculate the gradient errors of the loss function with the model's parameters. These gradients are used to update the parameters and optimize the model. The loss function can be expressed as

$$E_{Loss} = \frac{1}{n} \sum_{i=1}^{n} (t_i - y_i)^2, \tag{11}$$

where t_i is the target output and y_i is the network's prediction of the response i.

Batch normalization algorithm

The BN algorithm can compute the mean and variance of each neuron and then utilize these statistical values to normalize their inputs. This process allows each neuron in the network to adapt to the training data better, so it can accelerate the convergence rate of the network training. The calculation can be described as

$$\hat{x}^{(k)} = \frac{x^{(k)} - E[x^{(k)}]}{\sqrt{Var[x^{(k)}]}}, \tag{12}$$

where $\hat{x}^{(k)} = Wh + b$ is the input of the neurons in the network. W is the weight of the current layer. h is the output of the previous layer, and b is the bias term.

The output changes the learned feature distribution after normalization, and the BN algorithm configures learnable reconstruction parameters with

$$y^{(k)} = \gamma^{(k)} \hat{x}^{(k)} + \beta^{(k)}. \tag{13}$$

When $\gamma^{(k)} = \sqrt{Var[x^{(k)}]}$ and $\beta^{(k)} = E[x^{(k)}]$, the network can recover the original learned features by the reconstruction transformation.

Improved 1DCNN

Traditional neural networks, such as Back Propagation (BP) networks, are computationally fast, but their fitting accuracy is low. Although it is possible to optimize the neural network by machine learning to improve accuracy, it increases the training time of the network. In addition, the traditional method to design antennas by neural networks needs to use the structural parameters of the antenna as network inputs. However, the antenna parameters have low feature dimensions and the neural network extracts the features to reduce the dimensions of the feature mapping after forward propagation, which is unsuitable for deeper learning. To address these problems, a 1DCNN-IPS model is proposed in this paper. 1DCNN-IPS improves the propagation structure of the network by using padding in the convolutional layers in such a way that the inputs to the deeper convolutional layers remain sufficiently informative. The network concludes with three convolutional layers, a max pooling layer, and a fully connected layer. Compared to the standard CNN model, the 1DCNN-IPS model scheme is as follows:

(i) Padding is added to the convolutional layer to mitigate the problem of the network losing information during forward propagation. The same padding is calculated as [25]

$$N = \frac{W - F + 2P}{S} + 1, \tag{14}$$

where N represents the output dimension and W represents the dimension of the input features. F represents the

https://doi.org/10.1017/S1759078725000303 Published online by Cambridge University Press

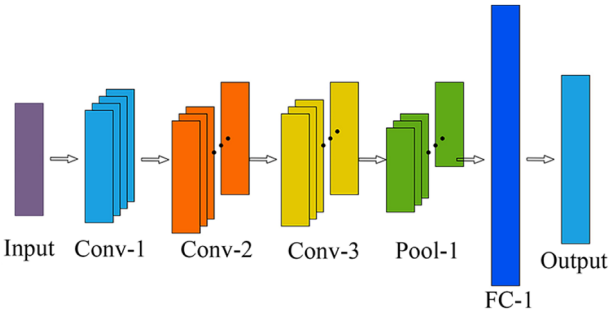


Figure 6. Structure of 1DCNN-IPS.

Table 2. The structure and parameter count of the 1DCNN-IPD model

Layer	Kernel size	Parameters
Input	–	–
Conv-1	2×1	24
Batchnorm-1	–	16
Relu-1	–	–
Conv-2	2×1	272
Batchnorm-2	–	32
Relu-2	–	–
Conv-3	2×1	1056
Batchnorm-3	–	64
Relu-3	–	–
Maxpool	2×1	–
FC	–	4128

dimension of the convolution kernel. S represents the step size, and P represents the number of padding layers;

(ii) The BN layer is added after each convolutional layer to adjust the distribution of the output of the convolutional layer;

(iii) The ReLU activation function between convolutional layers is explored instead of the Sigmoid function. It gives the neurons sparse activation and alleviates the vanishing gradient problem. The ReLU activation function is expressed as follows:

$$f_{\mathrm{ReLU}}(x) = \max(0, x). \tag{15}$$

The function returns 0 if it receives any negative input but returns it back for any positive value x.

The 1DCNN-IPS model concludes with three convolutional layers with a convolutional kernel size of two and a max pooling layer to extract features. Padding is added to the convolutional layers, and the BN layer is added after each convolutional layer. The ReLU activation function accelerates the model training, alleviating the problem of training overfitting and enhancing the model robustness. The structure of the 1DCNN-IPS model is shown in Fig. 6.

The network architecture and parameter count of the 1DCNN-IPS model designed in this paper are presented in Table 2. The model has approximately 5.5K computational parameters. In the case of optimal prediction performance, the parameter counts for 1DCNN, MLP, and 1DLeNet-5 networks are 5.6K, 5.8K, and 6.4K, respectively. Compared to these models, the model designed in this paper has fewer parameters.

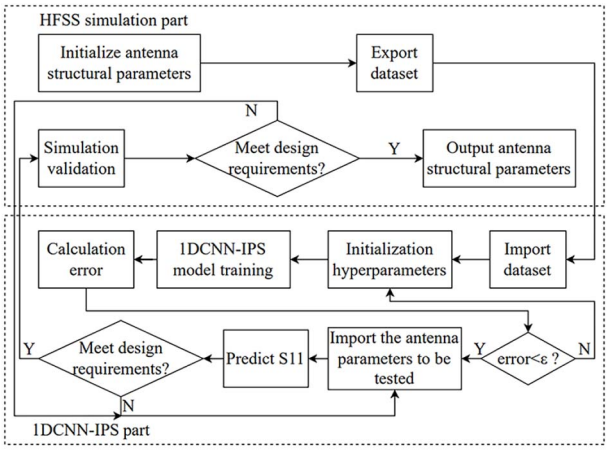


Figure 7. The 1DCNN-IPS optimized UWB antenna design flowchart.

Optimized design of UWB antennas by 1DCNN-IPS

Figure 4 shows that the structural parameters of the antenna's bent slot greatly impact the reflection coefficient. Optimizing with electromagnetic simulation software usually requires multiple simulation calculations, and each calculation takes a certain amount of time. Specifically for complex antenna structures, the time required for simulation calculations may be very long. In contrast, CNN can evaluate and optimize plenty of design schemes quickly. Upon completion of the training process, CNNs can promptly predict the performance of new design schemes, thereby leading to a significant reduction in the optimization cycle. Consequently, we use the 1DCNN-IPS model to optimize the antenna design. The 1DCNN-IPS optimized UWB antenna design flowchart is shown in Fig. 7.

The process consists of the HFSS simulation part and the 1DCNN-IPS network-based antenna bent slot optimization part. The HFSS simulation part mainly performs the following two functions:

(i) During the HFSS simulation, the antenna's structural parameters and reflection coefficients are obtained, providing a dataset for the subsequent training of the 1DCNN-IPS network.

(ii) Verify the accuracy of the antenna reflection coefficients output by the 1DCNN-IPS network.

The antenna bent slot optimization process based on the 1DCNN-IPS network primarily includes the following:

(i) Training the 1DCNN-IPS model using the dataset derived from the HFSS simulation part. The training procedure focuses on adjusting the model's parameters to accurately predict the relationship between the antenna's reflection coefficients and the structural parameters of the bent slot.

(ii) Once the network training is completed, the antenna parameters to be tested are imported, and the 1DCNN-IPS model is used for final performance prediction and verification. Subsequently, the optimal structural parameters of the bent slot are determined based on the reflection coefficient results.

https://doi.org/10.1017/S1759078725000303 Published online by Cambridge University Press

Table 3. Structural parameter range of the antenna

Parameter	Value (mm)
W4	3.55 : 0.1 : 4.05
L4	3.55 : 0.1 : 4.05
W5	2.55 : 0.1 : 3.05
Wd	0.4 : 0.1 : 0.5

It is important to note that HFSS simulations require significant computational time after modifying the antenna's structural parameters. However, once the 1DCNN-IPS network is trained, the corresponding reflection coefficient results can be immediately obtained by inputting the structural parameters of the bent slot into the network. Based on these reflection coefficient results, the structural parameters of the bent slot can be optimized, thereby saving the calculation time of using the HFSS software.

The detailed steps for optimizing the antenna's bent slot structure using 1DCNN-IPS are as follows.

(i) The antenna model is built using HFSS software, and the reflection coefficient parameters of the antenna are extracted by finite element method simulation. The output data are divided into training samples and testing samples with a ratio of 9:1. The structural parameters of the antenna are shown in Table 3.

(ii) The dataset is normalized, enabling equal scaling of the original data and unifying each parameter's specification. The normalization calculation can be expressed as

$$X_{norm} = \frac{X - X_{min}}{X_{max} - X_{min}}, \tag{16}$$

where X_{norm} is the normalized output. X_{max} and X_{min} are the maximum and minimum values of X, respectively.

(iii) Build the 1DCNN-IPS model. The network contains three convolutional layers, and padding has been added to improve the network structure. The BN layer is added after each convolutional layer to normalize its inputs and enhance the robustness of the network. The last convolutional layer connects the max pooling layer to speed up the computation.

(iv) Initialize the hyperparameters such as 1DCNN-IPS model weights w^l, bias b^l, loss function, training batch size, learning rate, etc.

(v) Train the 1DCNN-IPS model. The dataset obtained in Step (ii) is sent into the model. Once the model is trained well, it will calculate the error in the forward propagation phase and adjust the weight matrix in the backward propagation phase to optimize the network.

(vi) Optimization of the structural parameters of the bent slot. The trained model is employed to substitute the time-consuming electromagnetic simulation software for the optimization of the structural parameters of the bent slot. In contrast to the relatively long simulation time required by electromagnetic simulation software, the 1DCNN-IPS model can quickly establish the relationship between inputs and outputs. When the structural parameters of the bent slot are input into the model, the antenna's reflection coefficient is immediately output. If a notch exists in the reflection coefficient of the antenna within the WiMAX frequency band, and the antenna's frequency band meets the UWB design requirements, the structural parameters of the bent slot are recorded. If the results do not meet the design specifications, new parameters are selected for further testing.

(vii) Verification is performed using HFSS simulation. If the results do not meet the design requirements, the process returns to step (vi). If the requirements are met, the optimization of the antenna bent slot design is completed.

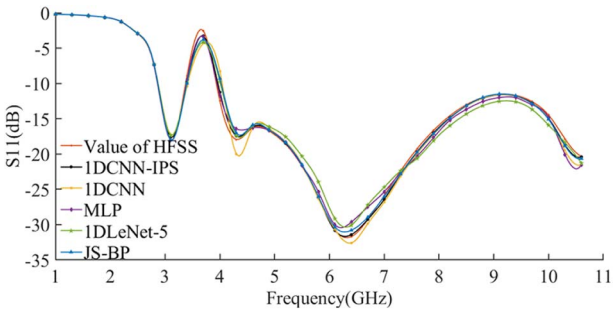


Figure 8. Prediction curves of the five models fitted to the HFSS simulation curves.

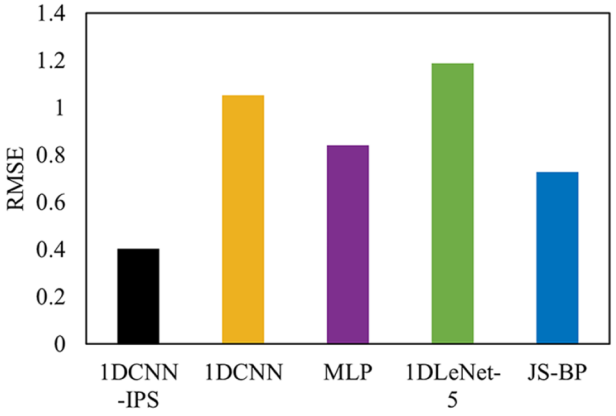


Figure 9. RMSE for five networks.

Experiments and analysis of results

This experiment was conducted in MATLAB R2022a to realize the construction and training of the five network models. The antenna designed in this paper was simulated using HFSS software, and the sweep range was set to 1–10.6 GHz with a step size of 0.3 GHz to derive the antenna reflection coefficient dataset. The 1DCNN-IPS model, 1DCNN model, MLP model, 1DLeNet-5 model, and Jellyfish Search-Optimized BP Neural Network JS-BP model were trained using the obtained dataset. After the training had been completed, the test set was used to verify the test effect of the five models.

As shown in Fig. 8, we compared the S11 prediction results of the 1DCNN-IPS model with the other four models. This figure shows that in the frequency band of 3.1–4.6 GHz, the 1DCNN model and and the 1DLeNet-5 model differ from the actual simulation results. In the frequency band 5.5–7 GHz, only the 1DCNN-IPS model can be fitted with the HFSS simulation results. As shown in the root mean squared error (RMSE) results in Fig. 9, the IDCNN-IPS model works better than the other four models.

The mean squared error (MSE) and running time of the five models are shown in Table 4. It can be seen that the MSE value of the 1DCNN-IPS model is 0.4342. The prediction accuracy of

https://doi.org/10.1017/S1759078725000303 Published online by Cambridge University Press

Table 4. Comparison of mse and computation time of different models

Model	MSE	Computation Time/sec
1DCNN-IPS	0.4342	16.5638
1DCNN	0.5602	16.0545
MLP	0.6003	18.2564
1DLeNet-5	0.5419	18.2367
JS-BP	0.6585	672.4004

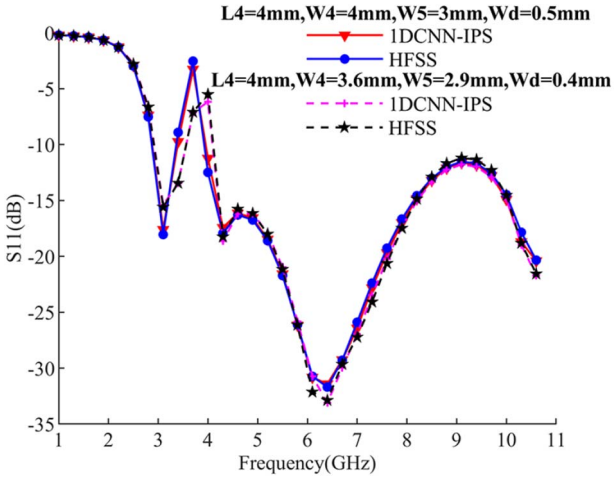


Figure 10. Effectiveness of 1DCNN-IPS fitting.

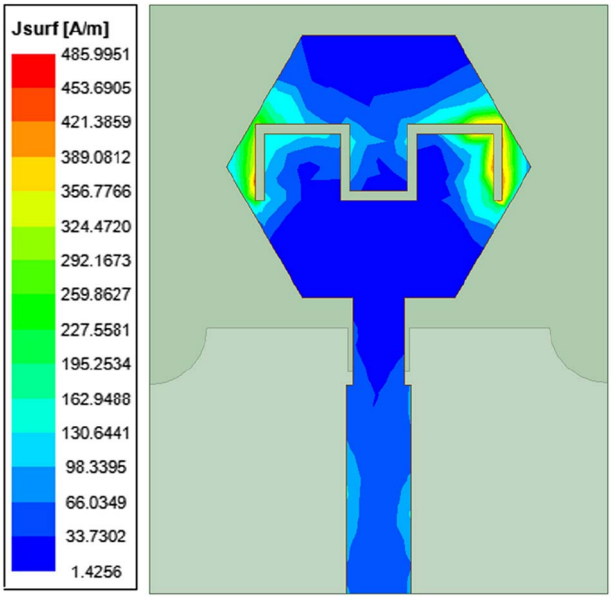


Figure 11. Antenna surface current distribution at 3.6 GHz.

the 1DCNN-IPS model is improved by 22.49%, 27.67%, 19.87%, and 34.06% than the 1DCNN model, MLP model, 1DLeNet-5 model, and JS-BP model, respectively. In terms of training time, the 1DCNN-IPS model is 9.17% faster than the 1DLeNet-5 model. So the 1DCNN-IPS model has lower MSE but faster computing speed.

The antenna structural parameters were optimized by using the trained 1DCNN-IPS model. The model inputs the structural

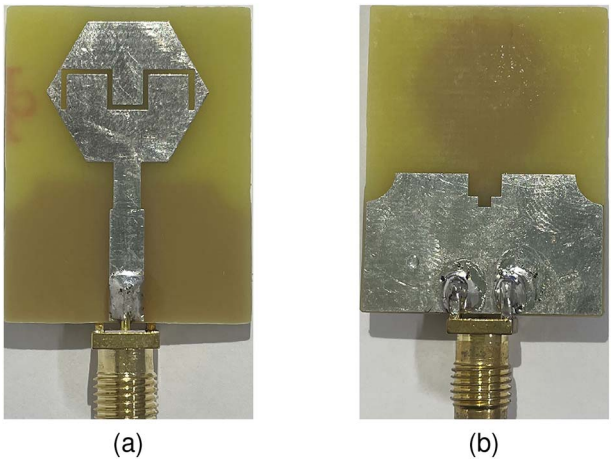


Figure 12. Prototype of the antenna. (a) Top view. (b) Bottom view.

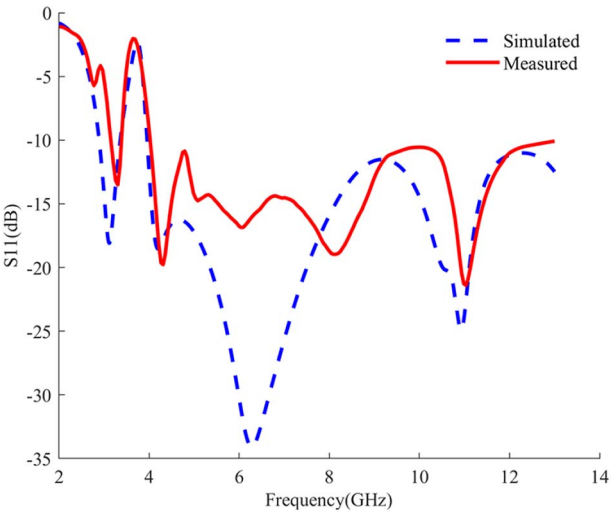


Figure 13. The simulation and measurement comparison of S11.

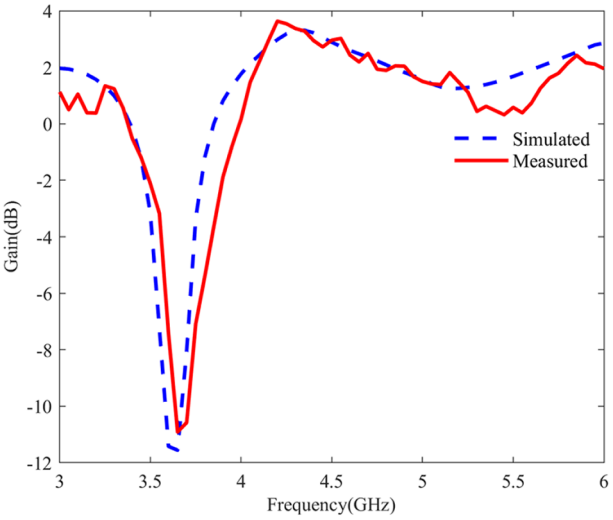


Figure 14. The measured and simulated gains of the antenna.

parameters of the antenna and outputs the reflection coefficient of the antenna. As shown in Fig. 10, if the lengths of L4, W4, W5,

https://doi.org/10.1017/S1759078725000303 Published online by Cambridge University Press

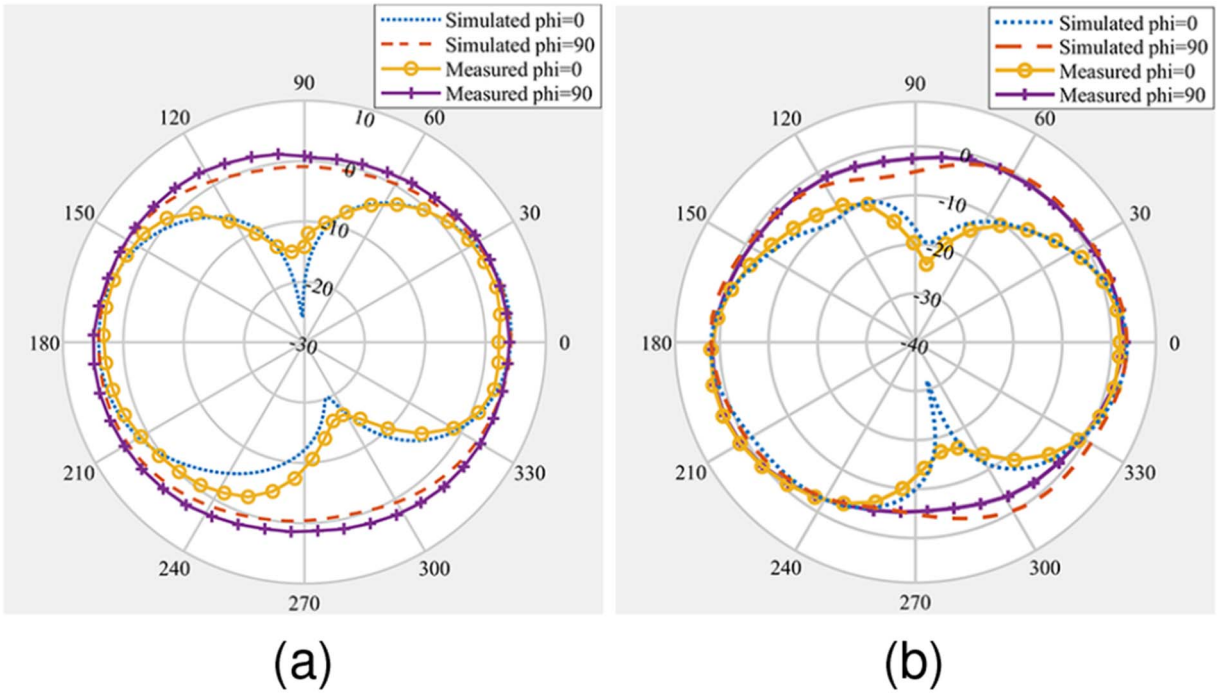


Figure 15. The radiation patterns of the antenna. (a) Radiation pattern at 4.5 GHz. (b) Radiation pattern at 9 GHz.

Table 5. Table of comparison between designed antenna and published work

Published work	Dimensions (mm^3)	Bandwidth (GHz)	Notched band (GHz)	Peak gain (UWB)(dBi)
[26]	$30 \times 35 \times 1.6$	2.16–12	3.34–3.76	2.2
[27]	$30 \times 30 \times 1.6$	3.9–10.7	–	–
[28]	$20 \times 28 \times 1.6$	2.5–8	3.3–3.8	2.29
Designed antenna	$24 \times 31 \times 1.5$	3.1–13	3.35–4	3.7

and Wd are 4 mm, 3.6 mm, 2.9 mm, and 0.4 mm respectively, the antenna's notched band will be 3.55–4.15 GHz, which does not satisfy the design requirements. If the four structural parameters are 4 mm, 4 mm, 3 mm, and 0.5 mm, respectively, the antenna's notched band is 3.3–3.9 GHz, which covers the work band of WiMAX. The antenna has an impedance bandwidth ($|S_{11}| < -10$ dB) from 2.8 to 14 GHz, which covers the entire UWB frequency band. Finally, after HFSS verification, the structural parameters of the antenna bent slot are set as L4 = 4 mm, W4 = 4 mm, W5 = 3 mm, and Wd = 0.5 mm.

According to the antenna band-notched principle, the antenna is further analyzed to determine the relationship between the bent slot and the corresponding notched band. By simulation, we obtain the antenna surface current distribution at the notch center with 3.6 GHz, as shown in Fig. 11. It can be seen that the current mainly gathers near the bent slot. A notched band is generated since the energy is pooled at the bent slot and cannot be radiated outward.

The physical diagram of the antenna is shown in Fig. 12. The antenna is manufactured on the FR4 substrate having dielectric constant $\varepsilon_r = 4.4$ and height $h = 1.5$ mm. After soldering the Radio Frequency (RF) coaxial connector (SubMiniature version A, SMA) joints, it was tested by using a vector network analyzer, and the results are shown in Fig. 13. Due to the errors in the fabrication process and the errors in soldering the SMA connector, etc., the simulated and measured results deviate from each other. From the measured waveforms, it can be seen that the antenna realizes the band-notched characteristic in the frequency band from 3.35 to 4 GHz. Except for the notched band, the reflection coefficient of the antenna is less than −10 dB, which can meet the UWB system's operation requirements.

Figure 14 shows the measured and simulated gain of the antenna in the WiMAX frequency band. As depicted in the figure, the antenna exhibits a noticeable decrease in gain in the WiMAX frequency band, effectively suppressing interference and impacts on narrowband communication bands.

The radiation characteristics of the band-notched UWB antenna are analyzed at 4.5 GHz and 9 GHz. Due to manufacturing errors in the antenna production process and the influence of the antenna testing environment, discrepancies occur between the testing and simulated results of the antenna. Simulated and measured Radiation Pattern for phi = 0 and phi = 90 are shown in Fig. 15. It is clear from Fig. 15 that the radiation pattern at lower frequency is omnidirectional while a little distortion at higher frequency is observed.

Table 5 presents the similarities and differences in various performances such as dimensions, bandwidth, notch band, and gain

https://doi.org/10.1017/S1759078725000303 Published online by Cambridge University Press

between the UWB notch antenna in this paper and the antennas in the references.

As shown in the table, the antenna designed in this study offers a wide bandwidth and exceptional notch characteristics. With its performance parameters, it is well-suited for a wide range of UWB applications. Compared with the works in the references, the proposed antenna demonstrates superior bandwidth, higher gain, and notch filtering capabilities. The antenna covers a frequency range from 3.1 to 13 GHz, with a notch band from 3.35 to 4 GHz, making it suitable for various UWB communication scenarios.

Conclusion

In this paper, a 1DCNN-IPS model is proposed to address the problem of the slow speed of multivariate optimization by EM software, and the bent slot structure is optimized by using this model. It is used alongside four other models to predict the reflection coefficient of the antenna. Experimental results show that the accuracy of the 1DCNN-IPS model is improved by 22.49%, 27.67%, 19.87%, and 34.06% over the 1DCNN model, MLP model, 1DLeNet-5 model, and JS-BP model, respectively. Additionally, the 1DCNN-IPS model demonstrates a 9.17% improvement in training time compared to the 1DLeNet-5 model. The 1DCNN-IPS model can widely optimize the bent slot structure and achieve the band-notched characteristic in the WiMAX of the antenna. It provides an effective tool for the rapid design of antennas. With its higher accuracy and improved prediction capability, the 1DCNN-IPS model is superior for optimized notched antenna modeling. The 1DCNN-IPS model inspires neural network designs capable of optimizing the structure of multi-notched band antennas in future work.

Acknowledgements. This work was supported by National Natural Science Foundation of China under Grant No. 62371245 and 62371248, National Key R&D Program of China (2023YFB2904000), Jiangsu Key Development Planning Project (BE2023004-2), Natural Science Foundation of Jiangsu Province (Higher Education Institutions) (20KJA520001), The 14th Five-Year Plan project of Equipment Development Department (315107402), and Jiangsu Hongxin Information Technology Co., Ltd Project.

Competing interests. The authors declare no potential conflict of interests.

References

1. **Zhu X, Yi J, Cheng J and He L** (2020) Adapted error map based mobile robot UWB indoor positioning. *IEEE Transactions on Instrumentation and Measurement* **69**(9), 6336–6350.
2. **Bastiaens S, Vanhie-Van Gerwen J, Macoir N, Deprez K, De Cock C, Joseph W, De Poorter E and Plets D** (2022) Experimental benchmarking of next-gen indoor positioning technologies (unmodulated) visible light positioning and ultra-wideband. *IEEE Internet of Things Journal* **9**(18), 17858–17870.
3. **Wu F and Liu Z** (2020) Research on uwb/imu fusion positioning technology in mine, Vientiane, Laos. In *2020 International Conference on Intelligent Transportation, Big Data & Smart City (ICITBS)*. IEEE, pp. 934–937.
4. **Rao PK and Mishra R** (2018) Multi Band Antenna with Multi Band Notch 2.5/3.7/6.4/8.1/12.4/14.4 GHz Characteristics, Gorakhpur, India. In *2018 5th IEEE Uttar Pradesh Section International Conference on Electrical, Electronics and Computer Engineering (UPCON)*. IEEE, pp. 1–5.
5. **Wei F, Li WT and Shi XW** (2012) Compact UWB bandpass filter with triple-notched bands using triple-mode stepped impedance resonator. *IEEE Microwave and Wireless Components Letters* **22**(10), 512–514.
6. **Nan J, Zhao J and Gao M** (2021) A compact 8-states frequency reconfigurable UWB antenna. *IEEE Access* **9**, 144257–144263.
7. **Zhao Z, Zhang C and Lu Z** (2023) A miniaturized wearable antenna with five band-notched characteristics for medical applications. *IEEE Antennas and Wireless Propagation Letters* **22**(6), 1246–1250.
8. **Tang Z, Wu X, Zhan J, Hu S, Xi Z and Liu Y** (2019) Compact UWB-MIMO antenna with high isolation and triple band-notched characteristics. *IEEE Access* **7**, 19856–19865.
9. **Awan WA, Zaidi A, Hussain N, Iqbal A and Baghdad A** (2019) Stub loaded, low profile UWB antenna with independently controllable notch-bands. *Microwave and Optical Technology Letters* **61**(11), 2447–2454.
10. **Li WT, Hei YQ and Feng W** (2012) Planar antenna for 3G/Bluetooth/WiMAX and UWB applications with dual band-notched characteristics. *IEEE Antennas and Wireless Propagation Letters* **11**, 61–64.
11. **Sanyal R, Coomar S, Sarkar DC, Bera PS and Sarkar PP** (2020) Design of UWB Monopole Antenna with 5.5/7.5 GHz Enhanced and Controllable Dual Band Rejection Characteristics, Kolkata, India. In *2020 IEEE 1st International Conference for Convergence in Engineering (ICCE)*. IEEE, pp. 325–329.
12. **Kumar OP, Kumar P and Ali T** (2021) A compact dual-band notched UWB antenna for wireless applications. *Micromachines* **13**(1), 12.
13. **Wei F, Zou XT and Wang XY** (2018) A differential UWB quasi–yagi antenna with a reconfigurable notched band. *Frequenz* **72**(9–10), 401–406.
14. **Lv Y, Zhang J and Hou H** (2019) A novel triple band-notched UWB printed monopole antenna. *Progress In Electromagnetics Research M* **81**, 85–95.
15. **Qi H and Liu H** (2021) Single-ended band-notched Vivaldi antenna with common mode suppression and low cross polarization. *IEEE Antennas and Wireless Propagation Letters* **20**(10), 1983–1987.
16. **Huang J, Li W, He Y, Zhang L and Wong SW** (2021) Optimization of antenna design using the ANN and the simulated annealing algorithm, Shenzhen, China. In *2021 Computing, Communications and IoT Applications (ComComAp)*. IEEE, pp. 119–122.
17. **Tian Y, Li N, Wang H, Li XP and Lee KY** (2016) Right-angled microcoaxial bends for Si-based RF/microwave integrated circuits. *IEEE Transactions on Components, Packaging and Manufacturing Technology* **6**(2), 290–297.
18. **Bouhous A** (2022) Prediction of resonance frequencies of rectangular patch antenna using a multilayer perceptron network, M'sila, Algeria. In *2022 5th International Symposium on Informatics and its Applications (ISIA)*. IEEE, pp. 1–4.
19. **Qin PY, Wei F and Guo YJ** (2015) A wideband-to-narrowband tunable antenna using a reconfigurable filter. *IEEE Transactions on Antennas and Propagation* **63**(5), 2282–2285.
20. **Singh AK, Dwivedi AK, Singh V and Yadav RS** (2021) A Miniaturized Planar Antenna with Optimized Slots and DGS for UWB Applications, Online. In *2021 International Conference Engineering and Telecommunication (En&T)*. IEEE, pp. 1–5.
21. **Sharma N and Bhatia SS** (2019) Design of printed monopole antenna with band notch characteristics for ultra-wideband applications. *International Journal of RF and Microwave Computer-Aided Engineering* **29**(10), e21894.
22. **Staszewski P, Jaworski M, Cao J and Rutkowski L** (2021) A new approach to descriptors generation for image retrieval by analyzing activations of deep neural network layers. *IEEE Transactions on Neural Networks and Learning Systems* **33**(12), 7913–7920.
23. **Pan M, Zhou H, Cao J, Liu Y, Hao J, Li S and Chen CH** (2020) Water level prediction model based on GRU and CNN. *IEEE Access* **8**, 60090–60100.
24. **Cheng H, Xie Z, Shi Y and Xiong N** (2019) Multi-step data prediction in wireless sensor networks based on one-dimensional CNN and bidirectional LSTM. *IEEE Access* **7**, 117883–117896.
25. **Simonyan K and Zisserman A** (2014) Very deep convolutional networks for large-scale image recognition. arXiv preprint arXiv:1409.1556.
26. **Malhotra H, Chaudhary N, Kumar N and Sharma M** (2021) Polygon Patch Antenna for Bluetooth And UWB Applications With Single Notch Rejection Characteristics, Noida, India. *9th International Conference on Reliability, Infocom Technologies and Optimization (Trends and Future Directions)(ICRITO)*. IEEE, pp. 1–5.

https://doi.org/10.1017/S1759078725000303 Published online by Cambridge University Press

27. **Jain R, Rana N and Ojha SS** (2023) A Tri-forked Antenna for UWB applications, Bhopal, India. *IEEE 12th International Conference on Communication Systems and Network Technologies (CSNT)*. IEEE, pp. 97–100.
28. **Choudhary N, Malhotra H, Kumar N and Sharma M** (2021) Polygon Patch Antenna For UWB And RADAR Applications With Notched Filter Characteristics Realized by inverted T-type stub, Noida, India. In *8th International Conference on Signal Processing and Integrated Networks (SPIN)*. IEEE, pp. 637–640.



Pengcheng Gao is currently pursuing a master's degree at Nanjing University of Posts and Telecommunications. His research interests include antennas and propagation.



Weigang Wang received his MS degree in Circuits and Systems from Nanjing University of Posts and Telecommunications in 2006 and the Ph.D. degree in Signal and Information Processing from Nanjing University of Posts and Telecommunications in 2015. His main research interests include wireless communication technology and signal processing.



Yuanjian Liu received his Ph.D. degree in Electromagnetic Field and Microwave Technology from Nanjing University of Posts and Telecommunications in 2009. His main research interests include Ray tracing methods and their engineering applications, indoor short-range wave propagation, and Indoor and outdoor wireless network coverage for complex environments.



Qijian Liu is currently pursuing a master's degree at Nanjing University of Posts and Telecommunications. His research interests include deep learning and image processing.



Yonghao Chen is currently pursuing a master's degree at Nanjing University of Posts and Telecommunications. His research interests include digital signal processing.



XiangMing Yan is currently pursuing a BS degree at Nanjing University of Posts and Telecommunications. Her research interests include embedded system design.

https://doi.org/10.1017/S1759078725000303 Published online by Cambridge University Press